Preferences of farmers increased mitigation potential of reforestation

J. Pongratz[1*], C.H. Reick[2], T. Raddatz[2], M. Claussen,[2,3] & K. Caldeira[1]

[1]*Department of Global Ecology, Carnegie Institution for Science, Stanford, USA. pongratz@carnegie.stanford.edu*

[2]*Max Planck Institute for Meteorology, Hamburg, Germany*

[3]*KlimaCampus, University of Hamburg, Hamburg, Germany*

The transformation from natural land cover to management ("anthropogenic land cover change", ALCC) has substantial influence on present-day surface temperatures. Clearing of forest for agriculture can cause CO_2 emissions[1] and therefore contribute to the greenhouse effect increasing global mean temperature[2]. However, ALCC can also increase surface albedo (reflectivity), which exerts a cooling influence[3,4]. Previous studies of idealized, large-scale deforestation[4–8] found that albedo cooling dominates over CO_2 warming in boreal regions, indicating that boreal reforestation is not an effective mitigation tool. Here we show that for historical land cover change in boreal regions, CO_2 warming dominated over albedo cooling because farmers chose to use the most productive land with larger carbon stocks and less snow than on average. The preferences of farmers extended CO_2 dominance to most agriculturally important regions in the world, so that the reversion of past land cover change should contribute to climate change mitigation in most places.

More than one third of the Earth's land surface has undergone ALCC, predominantly caused

by agricultural expansion. This has strongly influenced climate. On the one hand, ALCC alters biogeochemical cycles, most notably causes CO_2 emissions from loss of standing biomass with deforestation[1] and loss of soil carbon under management[9]. On the other hand, ALCC alters the biophysical properties of the land surface. In particular, the albedo of forest is usually lower than that of agricultural land, so that deforestation typically leads to less solar radiation being absorbed at the surface[4]. This is especially true in the presence of snow, which is "masked" by forest[3]. Exceptions include regions with dark soil that becomes exposed with deforestation, thus reducing surface albedo. While there is no consensus on the overall sign of the global temperature response to global historical ALCC[10–12], studies agree on a substantial warming from the biogeochemical effects[2], and usually a global cooling from biogeophysical effects, primarily driven by the increase in surface albedo[13].

The studies cited above have focused on the climate response to global ALCC. But the amount of CO_2 emissions and the change in biophysical properties vary across regions and types of land cover change. Simulating the climate response to global ALCC does therefore not reveal how much a specific local occurrence of ALCC altered global mean climate.

Knowing the contribution of local ALCC to global climate change is important for at least three reasons. First, this information is necessary to attribute causes of past climate change. Second, agricultural expansion will continue in some of the regions of past ALCC, with similar climatic consequences. Third, forestation has been suggested as a tool to mitigate global warming because a growing forest takes up and stores carbon from the atmosphere[14]. Studies[4,5] have how-

ever shown that in boreal regions warming caused by the reduction in surface albedo could dominate over the CO_2 uptake, i.e. the magnitude of the positive albedo forcing following forestation could be larger than the magnitude of the negative forcing from CO_2 uptake. This finding has subsequently been confirmed by further large-scale forestation/deforestation model experiments[6–8]. Under the constraints imposed by climate and the availability of area, a reversal of past ALCC may often be the most feasible step of implementing ALCC as mitigation tool. The climate effect of past ALCC indicates the mitigation potential of reversing the area to its natural state.

In this study, we quantify the contribution of local ALCC (Fig. 1) to historical global warming. To localize and compare biogeophysical and biogeochemical effects on climate we calculate radiative forcing (RF). RF is defined as the change in tropopause radiative fluxes caused by a climate perturbation prior to any feedbacks, a measure that ideally is proportional to a change in global mean surface temperature[15]. From transient climate simulations[16,17] with the comprehensive climate-carbon cycle model ECHAM5-JSBACH/MPIOM-HAMOCC5 we determine the increase in atmospheric CO_2 caused by ALCC and quantify the contribution of each individual grid cell to this CO_2 increase. We then compare the RF associated with the increase in CO_2 to the one from effects of surface albedo changes on radiative fluxes at the tropopause (see Method section). The time period covers the last millennium (AD 800 to 1992) and therefore much of the human impact on the climate system over the agricultural era[16,18].

The change in RF from surface albedo changes (Fig. 2a) has a global mean value of $-0.20\,\mathrm{W/m^2}$. The albedo RF has strongly negative values in Central and East Europe, where the greatest defor-

estation occurs, and in the tropical and subtropical regions, where a large albedo increase coincides with high insolation. Small positive values emerge over dark soils exposed by deforestation (e.g. central Asia) or bright soils more continuously covered by vegetation under management (e.g. Sahel). Fig. 2b depicts the mostly positive RF from CO_2 emissions since AD 800. Its global mean is 0.35 W/m^2 caused by an atmospheric CO_2 increase of 19 ppm. High RF is caused by deforestation in Europe and North America due to the large amounts of land area converted, but also by deforestation in the tropics and subtropics due to the large loss of standing biomass. The CO_2 RF and albedo RF sum to a global total RF value of 0.15 W/m^2. The regions with the most intense large-scale cultivation worldwide — Europe, India, China, and Eastern North America — and regions with tropical forest have a positive total RF. Smaller areas of negative RF are found in the western U.S., subtropical regions, Australia, and central south Asia, often agriculturally more marginal regions where grasslands and shrublands are used for pasture.

The relative importance of CO_2 and albedo in causing a positive or negative total RF is detailed in Fig. 3. ALCC has had a warming influence in the majority of places. Positive CO_2 RF dominates over negative albedo RF over about half of Earth's land surface; these areas include the regions of strongest total RF from ALCC. Total RF from ALCC in many snowy boreal regions is indeed negative and albedo-dominated, but these tend to be areas with little agriculture and thus have small total RF. Other areas in which ALCC has caused a negative total RF occur mainly for two reasons. In some locations, such as in parts of the western U.S., CO_2 warming is overcompensated by albedo cooling, often because a strong albedo increase due to bright soils coincides with low emissions from grassland and shrubland conversion. In other locations, such as in parts

of Australia, increase in carbon stocks and increase in albedo both act as cooling influence. Indeed, past ALCC may in some cases have led to carbon uptake, in particular for transformation to pasture, which can result in an accumulation of high amounts of soil organic carbon; sequestration strengths however depend on field-level management[9], an aspect not accounted for in our model.

The historical analysis presented here indicates the likely global climate impact of continuing deforestation. Currently, rates of net deforestation are highest in the tropics[19], regions in which, in our analysis, effects of CO_2 clearly dominate. Our regional assessment is consistent with previous simulations suggesting global warming from hypothetic large-scale tropical deforestation[4,7], but also shows the spatial heterogeneity of these regions in the relative importance of CO_2 emissions and surface albedo aspects (Fig. 3). Conversely, agricultural areas are being abandoned in many extra-tropical regions, in particular in North America and Europe[20]. It has been suggested to use these areas for biofuel production rather than to revert them to their natural vegetation cover. Fig. 3 suggests regions such as the western U.S. in which the strong negative RF from surface albedo changes has been offset only slightly by the positive RF from changes in carbon stocks. Keeping such areas under agricultural use will therefore contribute to mitigating global warming.

The dominance of CO_2 over albedo forcing applies to most areas with ALCC in the northern temperate and boreal regions. This contrasts with the findings of previous studies that albedo effects dominate in these regions[4–8]. The reason for the apparent discrepancy to previous modeling studies lies in the assumption of the underlying land cover change. In these largely idealized studies whole latitude bands of homogeneous forest cover were completely replaced by grasslands.

However, land cover change in the past happened preferentially in places most suitable for agriculture. Farmers usually used the most productive locations first, which implied above-average carbon stocks of the natural vegetation (Fig. 4a) and therefore high CO_2 emissions. Furthermore, within a vegetation zone, farmers preferred areas with less snow cover (Fig. 4b), so that the albedo change resulting from deforestation was smaller than would occur under mean snow conditions. If we assume that upon a reversal of historical ALCC the future carbon cycle would respond at a similar time scale as in the past, the effects of this reversal should be comparable in magnitude to Fig. 2c, but of opposite sign. Accordingly, reforestation even in high to midlatitudes would be expected to have a net cooling influence and thus could be an effective mitigation tool.

A CO_2 dominance for afforestation in the boreal region has been suggested by a satellite-based study[21], which assigned carbon stocks by vegetation type assuming values for boreal forest that were higher than simulated by most biosphere models. Our model predicts variations in carbon stocks within vegetation types with mean values consistent with most other assessments. In contrast to Montenegro et al.[21], we find that a primary reason for the boreal CO_2 dominance is the farmers' choice in the past to use regions with high carbon stocks, and not that previous model studies[4–8] have underestimated mean boreal forest carbon stocks.

Our results clearly depend on an accurate representation of the calculation of CO_2 and albedo RF and on their quality as temperature proxy. Our estimates of albedo RF and of CO_2 emissions are within the range of previous estimates[16,18]. The calculation of the CO_2 RF is sensitive to the reference CO_2 concentration (Equ. 1 in Method section), which so far has been the preindustrial

level. We repeat our calculations under a realistic CO_2 evolution that includes fossil-fuel burning. Due to a larger airborne fraction of ALCC emissions with concurrent fossil-fuel burning, the CO_2 RF is slightly greater. Thus, our conclusion of a dominance of CO_2 over albedo RF is robust.

The albedo effect is the dominant biogeophysical effect on the global scale[13]. Still, focusing only on surface albedo changes neglects a range of other biogeophysical effects of ALCC[22] that cannot be simply quantified as RF, so that their impact cannot be easily attributed to geographic locations. ALCC alters evapotranspiration, which is reduced particularly by deforestation. This leads to less water vapor in the atmosphere and a negative RF, which however has a substantially smaller magnitude than the negative albedo RF[23]. Moreover, the resulting cooling is counteracted by mechanisms that warm the surface, namely less evaporative cooling at the surface and a reduction in cloud cover associated with reduced evapotranspiration. Because these effects act in the same direction as the CO_2 RF, namely warming, the albedo effect likely constitutes an upper estimate of the cooling effect of biogeophysical changes. This further supports our conclusion of a dominance of CO_2 warming over biogeophysical effects.

The RF of future ALCC will depend on the future evolution of the climate system[5]. For a future reversion of ALCC, the scale of ALCC will influence the partitioning of CO_2 between atmosphere, ocean, and land. Detailed estimates of the effect of future ALCC would therefore depend on the specific climate and ALCC scenarios assumed. Nevertheless, our study suggests that in the past, most regions of intensive ALCC have contributed a positive forcing to global climate change because CO_2 effects dominate over albedo effects. The preferred choice in the past

was to use the most suitable areas for agriculture, which tended to have less snow cover and greater carbon stocks than average areas at the same latitude. These patterns are relevant for future land cover change in these areas, both for continued deforestation and a reversion to the natural state.

Method Summary

We perform transient simulations over the last millennium (years AD 800 to AD 1992) with the comprehensive climate-carbon cycle model ECHAM5-JSBACH/MPIOM-HAMOCC5 at approximately 4 degree spatial resolution[16]. We quantify the impact of global ALCC on the atmospheric CO_2 concentration by applying a detailed land cover reconstruction[24] as the only forcing. The contribution of each grid cell to present-day ALCC-induced CO_2 increase is quantified via the relative contribution to global emissions, taking into account that earlier emissions have been taken up to a larger part than recent emissions by applying a response function for the global land and ocean carbon pools. Contribution to atmospheric CO_2 is then translated to RF using the equation[25]

$$\Delta F_{CO_2} = 5.35\, W/m^2 \cdot ln(1 + \Delta C/C_0) \tag{1}$$

where C_0 is the average CO_2 concentration of the control simulation (281 ppm), and ΔC the increase in CO_2 caused by ALCC of a grid cell. As described above, we repeat this procedure applying fossil-fuel emissions in addition to ALCC as climate forcing. RF from surface albedo changes is calculated in equilibrium simulations for AD 800 and AD 1992[18]. At each time step in ECHAM5-JSBACH, we calculate radiative transfer twice to calculate surface albedo and tropopause radiative fluxes for the AD 800 and the AD 1992 land cover maps under exactly the same climate. This follows the definition of instantaneous RF[25], which excludes any climate feedbacks.

Acknowledgements The transient simulations for this study were carried out as part of the "Community Simulations of the Last Millennium" (http://www.mpimet.mpg.de/en/wissenschaft/working-groups/millennium.html); we would like to thank all participants.

Author Contributions JP, CHR, TR and MC designed the experiments, JP analyzed the simulation data. All authors contributed to designing the analysis and to writing the manuscript.

Author Information Correspondence should be addressed to J.P. (pongratz@carnegie.stanford.edu).

References

1. Houghton, R. *et al.* Changes in the carbon content of terrestrial biota and soils between 1860 and 1980: A net release of CO_2 to the atmosphere. *Ecol. Monogr.* **53**, 235–262 (1983).

2. Denman, K. *et al.* Couplings Between Changes in the Climate System and Biogeochemistry. In Solomon, S. *et al.* (eds.) *Climate Change 2007: The Physical Science Basis. Contribution of Working Group I to the Fourth Assessment Report of the Intergovernmental Panel on Climate Change* (Cambridge University Press, Cambridge, United Kingdom and New York, NY, USA, 2007).

3. Bonan, G., Pollard, D. & Thompson, S. Effects of boreal forest vegetation on global climate. *Nature* **359**, 716–718 (1992).

4. Claussen, M., Brovkin, V. & Ganopolski, A. Biogeophysical versus biogeochemical feedbacks of large-scale land cover change. *Geophys. Res. Lett.* **28**, 1011–1014 (2001).

5. Betts, R. Offset of the potential carbon sink from boreal forestation by decreases in surface albedo. *Nature* **408**, 187–190 (2000).

6. Sitch, S. *et al.* Impacts of future land cover changes on atmospheric CO_2 and climate. *Global Biogeochem. Cycles* **19**, GB2013, doi:10.1029/2004GB002311 (2005).

7. Bala, G. *et al.* Combined climate and carbon-cycle effects of large-scale deforestation. *PNAS* **104**, 6550–6555 (2007).

8. Bathiany, S., Claussen, M., Brovkin, V., Raddatz, T. & Gayler, V. Combined biogeophysical and biogeochemical effects of large-scale forest cover changes in the mpi earth system model. *Biogeosci.* **7**, 1383–1399, doi:10.5194/bg–7–1383–2010 (2010).

9. Guo, L. & Gifford, R. Soil carbon stocks and land use change: a meta analysis. *Global Change Biol.* **8**, 345–360 (2002).

10. Brovkin, V. *et al.* Role of land cover changes for atmospheric CO_2 increase and climate change during the last 150 years. *Global Change Biol.* **10**, 1253–1266 (2004).

11. Matthews, H., Weaver, A., Meissner, K., Gillett, N. & Eby, M. Natural and anthropogenic climate change: incorporating historical land cover change, vegetation dynamics and the global carbon cycle. *Clim. Dyn.* **22**, 461–479 (2004).

12. Pongratz, J., Reick, C., Raddatz, T. & Claussen, M. Biogeophysical versus biogeochemical climate response to historical anthropogenic land cover change. *Geophys. Res. Lett.* **37**, L08702, doi:10.1029/2010GL043010 (2010).

13. Betts, R. Biogeophysical impacts of land use on present-day climate: near-surface temperature change and radiative forcing. *Atmos. Sci. Lett.* **1**, doi:10.1006/asle.2001.0023 (2001).

14. United Nations Framework Convention on Climate Change (UNFCCC). *Reducing emissions from deforestation in developing countries: approaches to stimulate action* (2007). URL `http://www.unfccc.int/resource/docs/2005/cop11/eng/misc01.pdf`.

15. Hansen, J., Sato, M. & Ruedy, R. Radiative forcing and climate response. *J. Geophys. Res.* **102**, 6831–6864 (1997).

16. Pongratz, J., Reick, C., Raddatz, T. & Claussen, M. Effects of anthropogenic land cover change on the carbon cycle of the last millennium. *Global Biogeochem. Cycles* **23**, GB4001, doi:10.1029/2009GB003488 (2009).

17. Jungclaus, J. *et al.* Climate and carbon-cycle variability over the last millennium. *Clim. Past Discuss.* **6**, 1009–1044, doi:10.5194/cpd–6–1009–2010 (2010).

18. Pongratz, J., Raddatz, T., Reick, C., Esch, M. & Claussen, M. Radiative forcing from anthropogenic land cover change since A.D. 800. *Geophys. Res. Lett.* **36**, L02709, doi:10.1029/2008GL036394 (2009).

19. FAO. Global forest resources assessment 2005. *Main Report FAO forestry paper 147 (Rome: Food and Agriculture Organization of the UN)* pp. 320 (2005).

20. Campbell, J., Lobell, D., Genova, R. & Field, C. The global potential of bioenergy on abandoned agriculture lands. *Environ. Sci. Technol.* **42**, 5791–5794 (2008).

21. Montenegro, A. *et al.* The net carbon drawdown of small scale afforestation from satellite observations. *Glob. Planet. Change* **69**, 195–204 (2009).

22. Pielke, R., Sr. *et al.* The influence of land-use change and landscape dynamics on the climate system: relevance to climate-change policy beyond the radiative effect of greenhouse gases. *Phil. Trans. R. Soc. Lond. A* **360**, 1705–1719 (2002).

23. Davin, E., de Noblet-Ducoudré, N. & Friedlingstein, P. Impact of land cover change on surface climate: Relevance of the radiative forcing concept. *Geophys. Res. Lett.* **34**, L13702 (2007).

24. Pongratz, J., Reick, C., Raddatz, T. & Claussen, M. A reconstruction of global agricultural areas and land cover for the last millennium. *Global Biogeochem. Cycles* **22**, GB3018, doi:10.1029/2007GB003153 (2008).

25. Myhre, G., Highwood, E., Shine, K. & Stordal, F. New estimates of radiative forcing due to well mixed greenhouse gases. *Geophys. Res. Lett.* **25**, 2715–2718 (1998).

Figure captions

Fig. 1 Change in natural vegetation cover due to agricultural expansion AD 800 to 1992. Solid colors indicate change in forest cover (fraction of grid cell), hatching indicates regions where on more than 40% of the grid cell natural grass- and shrubland has been converted to agriculture.

Fig. 2 Changes in radiative forcing (RF), ΔF, AD 800 to 1992. **a** RF from ALCC-induced surface albedo changes; **b** RF from ALCC-induced CO_2 emissions; **c** total RF as sum of (a) and

(b).

Fig. 3 Relative importance of CO_2 and surface albedo radiative forcing (RF). In both panels, the colors encode the ratio of CO_2 RF over albedo RF, and correspond to the angular direction in the scatterplot.

Fig. 4 Difference in climate-relevant properties of natural versus managed areas. a Total carbon stock and **b** annual mean snow depth of the temperate/boreal vegetation types in our simulations averaged over the entire area in AD 800 (gray bars) or only the area subsequently transformed to agricultural use (black bars). Asterisks indicate differences between means of entire and used areas that are significant on the 95% level of a weighted two sample t-test.

Methods

Radiative forcing (RF) calculations. In the case of anthropogenic land cover change (ALCC), RF[25,26] is usually separated into the RF of the associated CO_2 emissions[27] and the RF from changes in surface albedo meant to represent the major biogeophysical effects[13,28]. For the albedo RF we perform calculations[18] with the land surface scheme JSBACH[29] coupled to the climate model ECHAM5[30] under present-day climate conditions. Simulations are performed for the years AD 800 and 1992 applying a historical land cover reconstruction[24]. At each time step, we calculate radiative transfer twice in ECHAM5-JSBACH to allow for calculation of surface albedo and tropopause radiative fluxes for the land cover maps of AD 800 and AD 1992 under exactly the same climate. This follows the definition of instantaneous RF[25], which excludes any feedbacks of climate.

For the CO_2 RF, we determine each grid cell's contribution to the present-day atmospheric CO_2 increase that is caused by ALCC. To do so, we rely on our previous estimates of ALCC-induced CO_2 emissions and the associated changes in atmospheric CO_2[16]. These use ECHAM5-JSBACH coupled to the ocean model MPIOM[31]/HAMOCC5[32] in transient simulations over the last millennium. ALCC-induced CO_2 emissions, i.e. gross emissions prior to any uptake by atmosphere, ocean, and land, are calculated from an additional offline simulation of the carbon pools. This offline simulation recalculates, for the ALCC scenario, the carbon pools under the climate of the control simulation, which is not affected by ALCC. The difference in carbon pool content between this offline and the control simulation quantifies gross emissions. The contribution of each grid cell to atmospheric CO_2 increase is determined via the relative contribution of each grid cell to global emissions. Because the ocean and land carbon pools take up emissions over time, early emissions will contribute less to present-day CO_2 increase than recent ones. To take this into account, we base the contribution to atmospheric CO_2 increase not on cumulative emissions, but on the integral of a convolution of the CO_2 emissions with a response function that represents the global sinks (see below).

The resulting grid cell emissions are finally translated into the RF from CO_2 emissions using the equation[25]

$$\Delta F_{CO_2} = 5.35\ W/m^2 \cdot ln(1 + \Delta C/C_0)\ . \tag{2}$$

Here, C_0 is the average CO_2 concentration of the control simulation (281 ppm), and ΔC the increase in CO_2 caused by ALCC of a grid cell. We eliminate the small error introduced on the global scale due to the non-linearity of the equation (3%) by scaling the grid cell emissions corres-

pondingly.

Sensitivity of CO_2 RF. We perform two additional coupled simulations to assess the sensitivity of the CO_2 RF to the climatic boundary conditions and atmospheric CO_2: One simulates climate and CO_2 driven by ALCC as well as fossil-fuel emissions, the other deviates from this after 1860 (when fossil-fuel emissions first reach non-negligible values[33]) by allowing only fossil-fuel emissions as climate forcing, keeping land cover fixed at 1860. The difference isolates the effect of ALCC under realistic atmospheric CO_2 and defines a realistic CO_2 evolution to be alternatively used as C_0.

When a realistic CO_2 evolution is applied as reference instead of a constant preindustrial CO_2 level, a weaker RF is obtained (see Equ. 1). On the other hand, the increase in atmospheric CO_2 that is caused by ALCC is simulated to be larger when fossil-fuel emissions are included (17 instead of 13 ppm since AD 1860). In the simulations with higher emission rates, the ocean takes up carbon less efficiently. Furthermore, there is a greater amount of biomass on land. Both of these factors result in ALCC impacting atmospheric CO_2 concentrations more strongly in simulations with concurrent fossil-fuel CO_2 release. The resulting CO_2 RF from ALCC under the CO_2 evolution including fossil-fuel emissions is 0.39 W/m^2 instead of 0.35 W/m^2 under preindustrial CO_2 levels. Our conclusion that the total RF from ALCC is dominated by the CO_2 RF is therefore robust against our choice of C_0.

Carbon cycle response function. To approximate the response of the global ocean and land carbon pools to CO_2 emissions of single grid cells, we fit an exponential response function Z to the

atmospheric CO_2 increase of the coupled simulation and the gross emissions E:

$$Z(t) = a_0 + \sum_j a_j \cdot e^{-\frac{t}{\tau_j}} \tag{3}$$

$$C(t) = C(0) + \int_0^t Z(t-s) \cdot E(s) ds \tag{4}$$

where $C(t)$ is the atmospheric CO_2 concentration at time t. Note that Z(0) = 1 and therefore all emissions are in the atmosphere at the time step they occur. The constants a_j and the time constants τ_j are fitted to the simulated CO_2 evolution. $a_0 = (1 - \sum a_j)$. The best fit is found for the sum of three exponential terms with time constants τ_1, τ_2, and τ_3 of approximately 1 month, 15 years, and 247 years, and constants a_1, a_2, and a_3 of 0.30, 0.34, and 0.36.

References

26. Hansen, J. *et al.* Efficacy of climate forcings. *J. Geophys. Res.* **110**, D18104 (2005).

27. Forster, P. *et al.* Changes in atmospheric constituents and in radiative forcing. In Solomon, S. *et al.* (eds.) *Climate Change 2007: The Physical Science Basis. Contribution of Working Group I to the Fourth Assessment Report of the Intergovernmental Panel on Climate Change*, 129–234 (Cambridge University Press, Cambridge, United Kingdom and New York, NY, USA, 2007).

28. Myhre, G. & Myhre, A. Uncertainties in radiative forcing due to surface albedo changes caused by land-use changes. *J. Climate* **16**, 1511–1524 (2003).

29. Raddatz, T. *et al.* Will the tropical land biosphere dominate the climate-carbon cycle feedback during the twenty-first century? *Clim. Dyn.* **29**, 565–574 (2007).

30. Roeckner, E. *et al. The atmospheric general circulation model ECHAM5. Part I: Model description*, vol. 349 (Report, Max Planck Institute for Meteorology, Hamburg, Germany, 2003).

31. Marsland, S., Haak, H., Jungclaus, J., Latif, M. & Roeske, F. The Max-Planck-Institute global ocean/sea ice model with orthogonal curvilinear coordinates. *Ocean Model* **5**, 91–127 (2003).

32. Wetzel, P., Winguth, A. & Maier-Reimer, E. Sea-to-air CO_2 fluxes from 1948 to 2003. *Global Biogeochem. Cycles* **19**, doi:10.1029/2004GB002339 (2005).

33. Marland, G., Andres, B. & Boden, T. *Global CO_2 emissions from fossil-fuel burning, cement manufacture, and gas flaring: 1751-2005* (Carbon Dioxide Information Analysis Center, 2008).

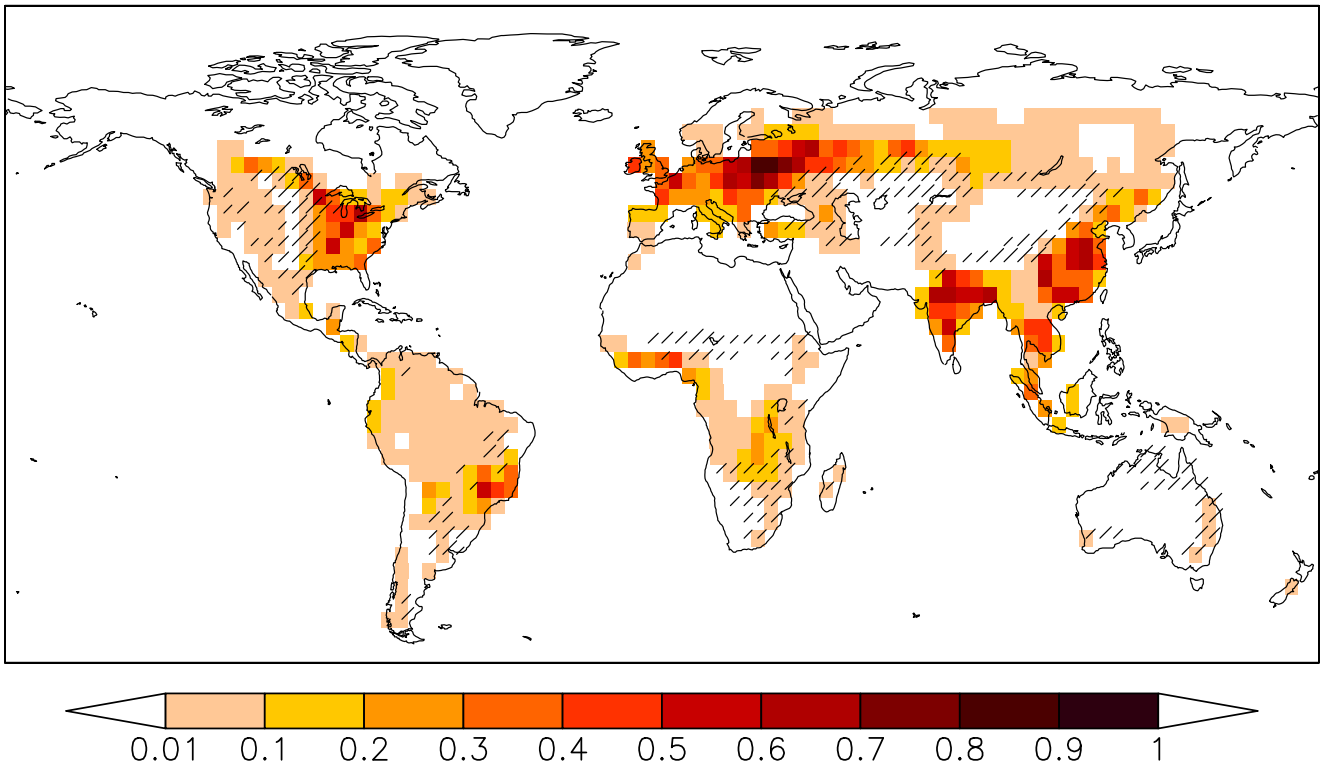
0.01
0.1
0.2
0.3
0.4
0.5
0.6
0.7
0.8
0.9
1

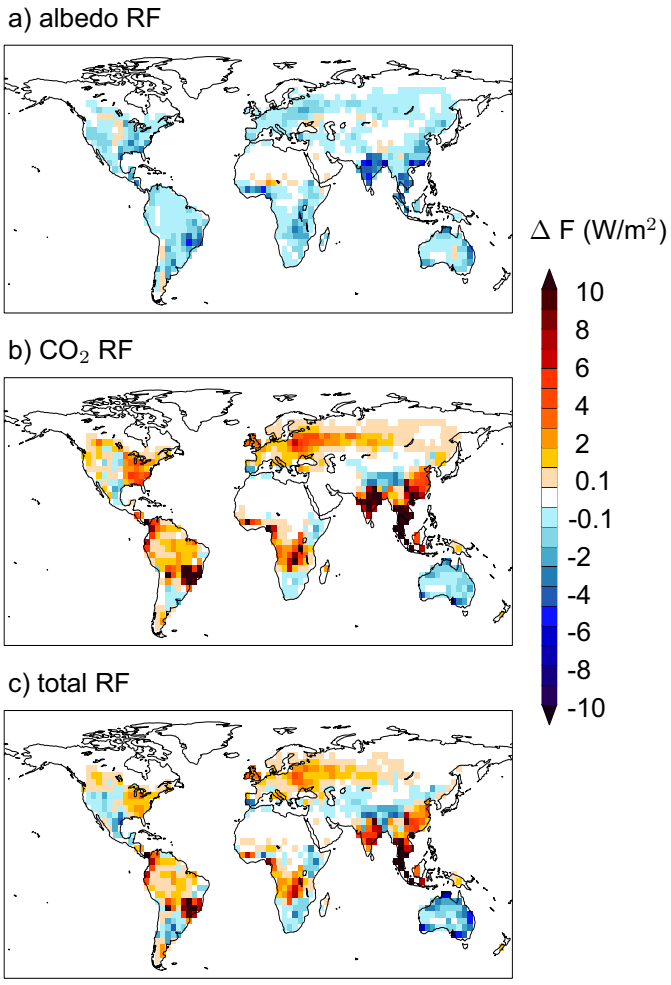
a) albedo RF
b) CO_2 RF
c) total RF
Δ F (W/m^2)
10
8
6
4
2
0.1
-0.1
-2
-4
-6
-8
-10

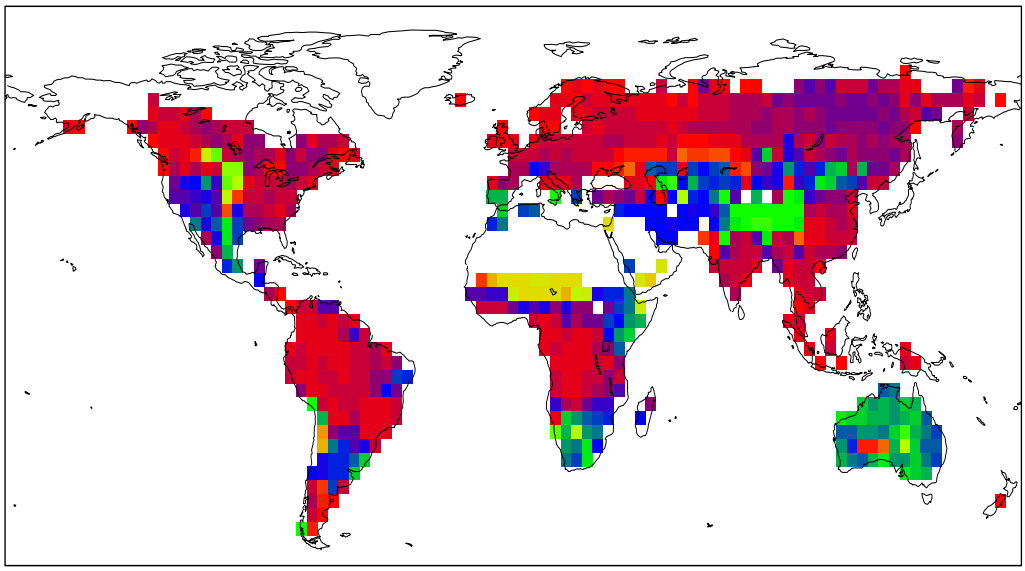

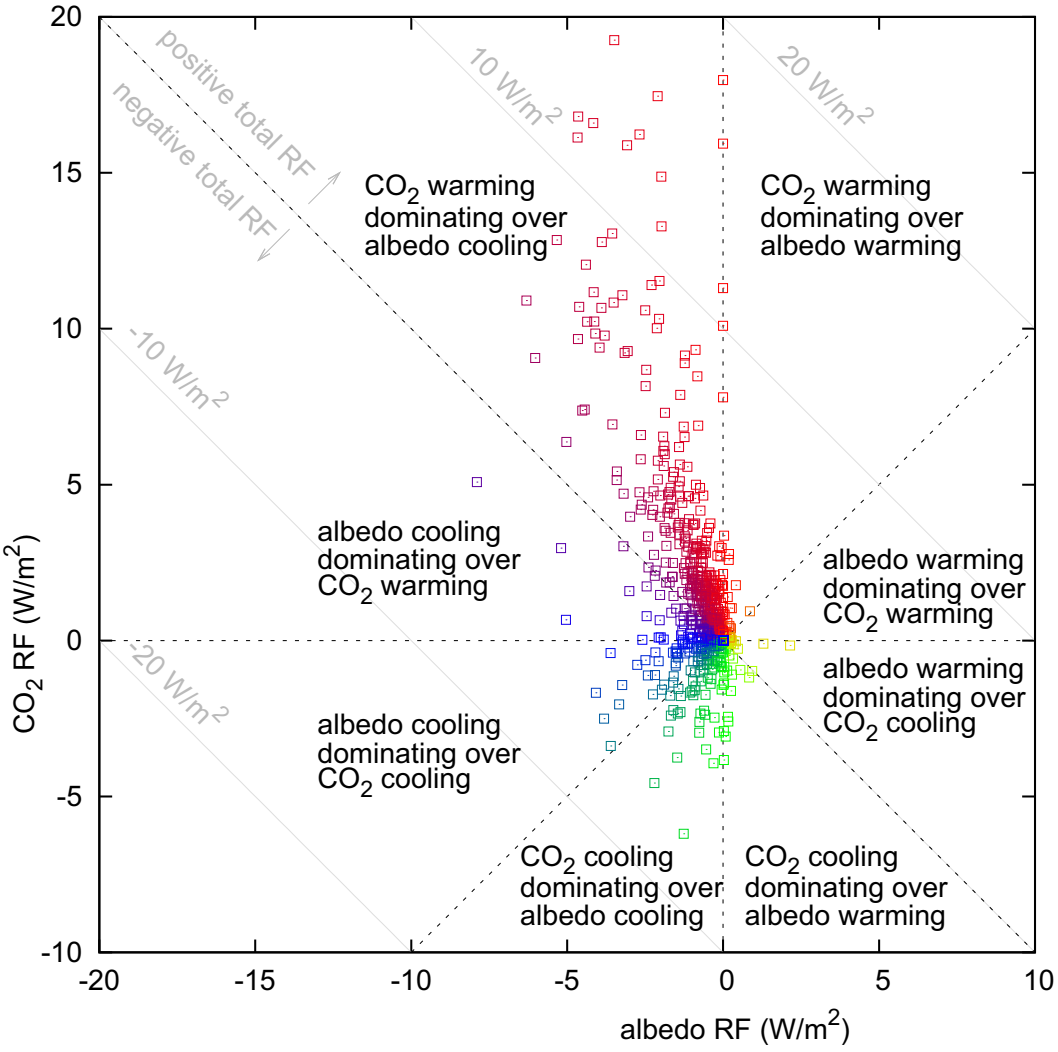
positive total RF
negative total RF
10 W/m2
20 W/m2
-10 W/m2
-20 W/m2
CO2 warming dominating over albedo cooling
CO2 warming dominating over albedo warming
albedo cooling dominating over CO2 warming
albedo warming dominating over CO2 warming
albedo warming dominating over CO2 cooling
albedo cooling dominating over CO2 cooling
CO2 cooling dominating over albedo cooling
CO2 cooling dominating over albedo warming
CO2 RF (W/m2)
albedo RF (W/m2)
20
15
10
5
0
-5
-10
-20
-15
-10
-5
0
5
10

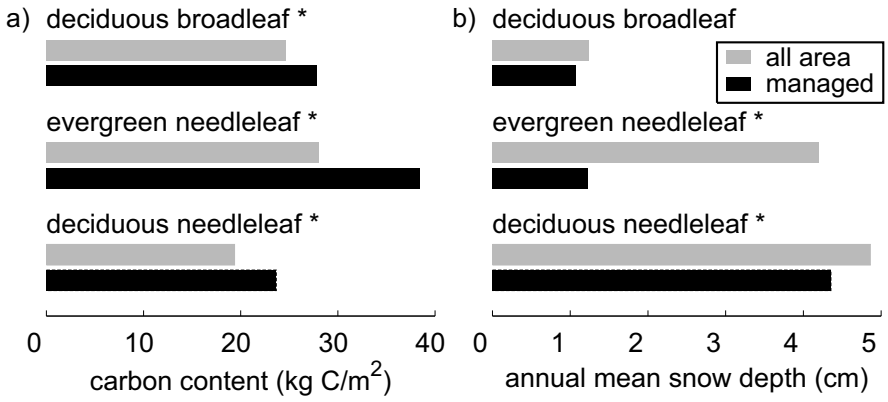
a)
deciduous broadleaf *
evergreen needleleaf *
deciduous needleleaf *
0
10
20
30
40
carbon content (kg C/m2)
b)
deciduous broadleaf
evergreen needleleaf *
deciduous needleleaf *
all area
managed
0
1
2
3
4
5
annual mean snow depth (cm)